A data-driven respiratory motion estimation approach for PET based on time-of-flight weighted positron emission particle tracking

Tasmia Rahman Tumpa[a)]
Graduate School of Medicine, The University of Tennessee, 1924 Alcoa Hwy, Knoxville, TN 37920, USA
Electrical Engineering and Computer Science, The University of Tennessee, 1520 Middle Dr, Knoxville, TN 37996, USA

Shelley N. Acuff
Graduate School of Medicine, The University of Tennessee, 1924 Alcoa Hwy, Knoxville, TN 37920, USA

Jens Gregor
Electrical Engineering and Computer Science, The University of Tennessee, 1520 Middle Dr, Knoxville, TN 37996, USA

Sanghyeb Lee
Independent Consultant, Novato, CA, USA

Dongming Hu
Independent Consultant, Knoxville, TN, USA

Dustin R. Osborne
Graduate School of Medicine, The University of Tennessee, 1924 Alcoa Hwy, Knoxville, TN 37920, USA

Purpose: Respiratory motion of patients during positron emission tomography (PET)/computed tomography (CT) imaging affects both image quality and quantitative accuracy. Hardware-based motion estimation, which is the current clinical standard, requires initial setup, maintenance, and calibration of the equipment, and can be associated with patient discomfort. Data-driven techniques are an active area of research with limited exploration into lesion-specific motion estimation. This paper introduces a time-of-flight (TOF)-weighted positron emission particle tracking (PEPT) algorithm that facilitates lesion-specific respiratory motion estimation from raw listmode PET data.

Methods: The TOF-PEPT algorithm was implemented and investigated under different scenarios: (a) a phantom study with a point source and an Anzai band for respiratory motion tracking; (b) a phantom study with a point source only, no Anzai band; (c) two clinical studies with point sources and the Anzai band; (d) two clinical studies with point sources only, no Anzai band; and (e) two clinical studies using lesions/internal regions instead of point sources and no Anzai band. For studies with radioactive point sources, they were placed on patients during PET/CT imaging. The motion tracking was performed using a preselected region of interest (ROI), manually drawn around point sources or lesions on reconstructed images. The extracted motion signals were compared with the Anzai band when applicable. For the purposes of additional comparison, a center-of-mass (COM) algorithm was implemented both with and without the use of TOF information. Using the motion estimate from each method, amplitude-based gating was applied, and gated images were reconstructed.

Results: The TOF-PEPT algorithm is shown to successfully determine the respiratory motion for both phantom and clinical studies. The derived motion signals correlated well with the Anzai band; correlation coefficients of 0.99 and 0.94-0.97 were obtained for the phantom study and the clinical studies, respectively. TOF-PEPT was found to be 13–38% better correlated with the Anzai results than the COM methods. Maximum Standardized Uptake Values (SUVs) were used to quantitatively compare the reconstructed-gated images. In comparison with the ungated image, a 14–39% increase in the max SUV across several lesion areas and an 8.7% increase in the max SUV on the tracked lesion area were observed in the gated images based on TOF-PEPT. The distinct presence of lesions with reduced blurring effect and generally sharper images were readily apparent in all clinical studies. In addition, max SUVs were found to be 4–10% higher in the TOF-PEPT-based gated images than in those based on Anzai and COM methods.

Conclusion: A PEPT- based algorithm has been presented for determining movement due to respiratory motion during PET/CT imaging. Gating based on the motion estimate is shown to quantifiably improve the image quality in both a controlled point source phantom study and in clinical data patient studies. The algorithm has the potential to facilitate true motion correction where the reconstruction algorithm can use all data available. © *2020 The Authors. Medical Physics* published by Wiley Periodicals LLC on behalf of American Association of Physicists in Medicine [https://doi.org/10.1002/mp.14613]

1. INTRODUCTION

Positron emission tomography (PET) is a noninvasive imaging modality widely used in clinical application to study organ and tissue function and is used most often in conjunction with computed tomography (CT) to acquire anatomical information and for emission data correction. Motion artifacts caused by the natural breathing of the patient during a scan are a major concern. Along with blurring and otherwise degraded image quality, motion artifacts may result in inaccurate localization of lesions, miscalculation of standardized uptake values (SUVs), and overestimation of tumor size and involvement.[1] Respiratory motion is particularly problematic for PET due to typical scan times of 2–5 min (8–20 min for whole-body scans), leading to averaging of the image pixel values across the range of motion.

The current clinical standard uses external measuring devices to extract respiratory signals from the patient. Dawood et al.,[2] Qiao et al.,[3] Lamare et al.,[4] and Liu et al.[5] presented methods using external devices. However, key issues exist related to device cost, service, maintenance, and more. The difficulties and the expense associated with the use of external measuring devices have resulted in an increased focus on data-driven methods for PET motion correction. Such methods provide a means to determine global (or external) motion as well as lesion-specific (internal) motion. This ability is important for proper quantification of lesions since internal motion may not perfectly match the external motion typically monitored.

To date, a wide range of data-driven approaches have been studied including center-of-mass (COM) methods proposed by Klein et al.[6] and Bundschuh et al.,[7] principal component analysis (PCA) by Thielemans et al.,[8] spectral analysis by Visvikis et al.[9] and Schleyer et al.,[10,11] sinogram region fluctuation (SRF) by Kesner et al.,[12,13] geometric sensitivity gating (GSG) by He et al.,[14] and combinations of different methodologies by Büther et al.[15,16] and others. None of these earlier papers considered time-of-flight (TOF)[17,18] information. With modern scanners, TOF information can play an important role in improving the data-driven motion estimation as evident by more recent COM algorithms by Ren et al.,[19,20] Lu et al.,[21] Xu et al.,[22] Feng et al.,[23] and Salomon et al.,[24] PCA techniques by Bertolli et al.[25,26] and Walker et al.,[27] and a combination thereof by Wang et al.[28,29] Except for a few of these papers,[19–21] only axial motion estimation was demonstrated. None of the papers reported on motion estimation for specific lesions.

Our aim is to study a modified version of the positron emission particle tracking[30–32] (PEPT) algorithm with application to lesion/internal region specific movement tracking due to respiratory motion. PEPT has been mostly used in industrial applications such as flow patterns[30,31] and velocity

measurements.[32] Other than our patent[33] and preliminary early work,[34–36] a variant of the PEPT algorithm was presented under the moniker positron emission tracking (PeTrack) for use in radiotherapy as well as cardiac PET studies using external markers.[37,38] PeTrack requires an initial estimate of the marker positions and has several user-defined threshold parameters. We modified the original PEPT algorithm to make its implementation data-driven and use TOF-based weighting. We refer to the resulting algorithm as TOF-PEPT and show its application using respiratory PET/CT data.

Our overall contributions are as follows: (a) proposing a PEPT-based data-driven motion tracking technique for estimating both external and internal motion signals due to respiratory motion; (b) utilizing TOF information to introduce weighting factors into the algorithm and determine control parameters; (c) applying the TOF-PEPT algorithm to list-mode data to estimate motion signals subsequently used for gating; (d) validating our recommendation of TOF-based weighting factors; and (e) validating the performance of the TOF-PEPT algorithm using the Anzai band while comparing against the COM algorithm by Ren et al.[19]

2. MATERIALS AND METHODS

2.A. Time-of-flight-based positron emission particle tracking (TOF-PEPT)

The PEPT algorithm estimates the location of a radioactive tracer particle by iteratively determining the point in space for which the sum of distances to a set of LORs is minimized. For the idealized case of a single radioactive tracer particle with no radioactive background, all LORs are expected to intersect at the location of the tracer. In reality, many LORs represent random events and Compton scattering. Also, emitted positrons travel a finite range before annihilation. All these lead to uncertainties in measuring the accurate location of the tracer particle. The PEPT algorithm aims at obtaining the location estimate by iteratively keeping a fraction of LORs which is more likely to provide a truer estimate.

Mathematically, let $L_i \in \Omega$ be the set of LORs considered for the current iteration, and let $\delta(L_i, p)$ represents the perpendicular distance from a specific LOR, L_i to some point p. The particle location is then estimated as

$$p_m = \mathrm{argmin}_p \sum_{L_i \in \Omega} \delta(L_i, p) \qquad (1)$$

LORs, for which the distances to p_m exceed the mean distance of the set by a user-defined threshold, are discarded before the process is repeated. The iteration stops when less than a pre-specified fraction of the initial set of LORs remains.

We have modified the PEPT algorithm to incorporate TOF-based weighting of the point distance, use of squared distance to solve the problem analytically, and use of data-driven rules for discarding LORs and stopping the iteration.

TOF information is commonly used in PET to narrow down the location of an emission event.[17] The location of the annihilation along an LOR can be determined by examining the differences in the TOF of each gamma ray. The location estimate is associated with an uncertainty σ_T that can be modeled by a Gaussian, whose FWHM is a function of the system coincidence timing resolution. For the Biograph mCT (Siemens Healthineers, USA), the timing resolution has been reported to be 527–580 ps[28,39–41] with lower values possible for individual LORs.[42]

The proposed TOF-PEPT algorithm uses σ_T to define a weighting factor for each LOR as well as to obtain a statistically based stopping criterion. That is,

$$p_m = \mathrm{argmin}_p \sum_{L_i \in \Omega} w_i \delta^2(L_i, p) \qquad (2)$$

where

$$w_i \triangleq 1 + \max\left\{0, 1 - \left(\frac{||p_i - p_m||}{\sqrt{2}\sigma_T}\right)^2\right\} \in [1, 2] \qquad (3)$$

Here, p_i denotes the TOF estimate of the annihilation location for L_i. The weighting factor, which is based on a first-order Taylor series expansion of a Gaussian function, places higher emphasis (up to 2x) on LORs for which the annihilation event is close to the current estimate of p_m than LORs that are further away (1x). We chose the weighting factors to be in the range of [1, 2] so that all the selected LORs contribute to the location estimate with the more probable LORs carrying more weight. The definition of the weighting factor is validated by the results presented in Sections 3.C and 4.

For the results reported below, we used $\sigma_T = 6.53$ cm based on an idealized individual LOR timing resolution of 512 ps. At the end of each iteration, we discard LORs, whose distances to the new point estimate are farther than 1 standard deviation away from the mean distance of the set. The iteration stops when the number of LORs kept drops below the number of LORs for which the TOF-based emission locations are within a sphere of radius σ_T surrounding the particle location estimate.

2.B. Method implementation and data processing

A PET scan can produce millions of LORs with emissions originating from many locations within the patient. In order to perform the computation on a specific region, we implemented a user-based selection of the ROI that limits which LORs will be considered during the computation. A graphical user interface was developed in MATLAB to allow visualization of DICOM files and to enable manual drawing of a box-shaped ROI around the source of interest. DICOM images were reconstructed using Biograph mCT (Siemens Healthineers, USA) software for a pixel size of 4.0728 mm ×

4.0728 mm with a slice thickness of 2.0084 mm. Each ROI was drawn by visual inspection to be approximately two to three pixels larger on each side than the source of interest. The size and location of the ROIs were mapped to the scanner geometry to facilitate LOR selection.

The listmode data was divided into chronological time frames of 500 ms. The TOF-PEPT algorithm was then applied to each time frame to estimate movement. Plotted as a function of time, the frame particle location provided motion signals along X, Y, and Z directions for the duration of the scan; below, we denote Left–Right (LR), Anterior–Posterior (AP), and Superior–Inferior (SI) directions by X, Y, and Z, respectively. The motion signal was smoothed by a low pass filter, the cutoff frequency of which was determined from the frequency corresponding to the peak magnitude.[19] The peak frequency magnitude varied from patient to patient ranging from ~0.167 to 0.3 Hz for the data studied.

2.C. Validation and evaluation

For gold standard comparison, we used a clinically approved respiratory band (Anzai Medical, Japan) which provided motion information related to inspiration and expiration. Comparison against another data-driven method was based on the COM algorithm proposed by Ren et al.[19]. To ensure a fair comparison, the COM algorithm was implemented using the same ROI restriction methodology as used for TOF-PEPT. We compared against COM using TOF (referred to as TOF-COM) and COM without using TOF (referred to as COM).

A quantitative comparison of the motion signals extracted by the TOF-PEPT and COM algorithms was performed against the gold standard Anzai band results. The analysis was conducted by calculating the following quality control measurements: Pearson correlation coefficient (CC),[13] root mean square error (RMSE), and mean shift in the peak location. To conduct the comparison, tracked data were resampled at the Anzai band sampling rate (20 ms) using MATLAB built-in "resample" function. The mean shift in peak location was calculated by taking the mean of shifts in peak locations w.r.t. the Anzai band data for each cycle normalized by the corresponding cycle duration of the band data.

Additionally, CC was used to study the performance of TOF-PEPT with and without the TOF-based weighting proposed in this paper as well as with and without the TOF-based LOR exclusion proposed for the PeTrack method. The latter discards LORs for which the distance from the TOF-based annihilation location to the current estimate of the particle location exceeds a user-defined threshold.[37,38]

To further validate our method, respiratory gating was implemented using the motion signals from each method. Amplitude-based gating is a widely practiced approach[43] and we adopted the gating in a way where for each individual cycle, all events that lie within the baseline amplitude to the 35% of the peak amplitude were kept. Using Biograph mCT software and the e7 processing tooling, the listmode data were rebinned into sinograms, which were then processed by

the manufacturer provided OSEM algorithm [with three iterations, 24 subsets, 5 mm Gaussian filter, UltraHD (TOF + PSF)] found on the mCT Flow PET/CT platform. The final reconstructed image corresponded with the phase of the cycle where the object statistically spent the greatest amount of time during the acquisition (usually the point of expiration for most patients). Using RadiAnt[44] and Inveon Research Workplace visualization software (Siemens Healthineers, USA), ROIs were drawn on the gated images to quantitatively compare data and assess the impact of motion correction. The images had the same resolution as the DICOM images mentioned previously.

Lastly, we assessed sensitivity of the TOF-PEPT algorithm to changes in the key user-defined parameters, namely, frame duration and ROI size. These two parameters control how many, and which, LORs are kept for each frame. The assessment focused on how the quality control measurements described above varied with the parameters. Five different frame durations of 200, 400, 600, 800, and 1000 ms were used. Controlled by the radius of the circumscribing sphere, the ROI was varied in size using scaling factors of 1.5, 2, and 2.75. Parameter sensitivity was studied for the TOF-PEPT algorithm only, as analysis for the COM algorithm was out of the scope of this work.

2.D. Data

Validation and performance evaluations were done using two phantom studies and six clinical studies. For the first phantom study, a single radioactive point source was attached to a respiratory phantom consisting of an elliptical disc rotating at a frequency of 0.18 Hz. The point source was placed on top of the platform, and the Anzai band was wrapped across the point source. The phantom exhibited the greatest range of movement in the Y direction (approximately 9–10 mm). The second phantom study was performed with a servo motor and a small arm attached to the motor. The motor was controlled using an Arduino board[45] which was programmed to move the arm up and down for 15 min at three different frequencies, namely, 0.167, 0.25, and 0.5 Hz, respectively for 7.5, 5, and 2.5 min with corresponding amplitude ranges of about 6, 3, and 1.5 mm in the Y direction. A point source was attached to the arm. The Anzai band was not used for this study.

The clinical studies were performed under the auspices of a University of Tennessee Graduate School of Medicine Institutional Review Board approved protocol (#3941). Patient imaging was performed on a 64-slice Biograph mCT Flow PET/CT using full 64-bit listmode data acquisition. We examined three scenarios each with two clinical studies. Clinical Studies 1 and 2 were conducted with the Anzai band placed on the abdomen using three radioactive point sources and one radioactive point source, respectively, attached close to the band. Clinical Studies 3 and 4 used a single point source each but no Anzai band. Clinical Studies 5 and 6 were performed solely using internal data, namely, the left cardiac ventricle and a ~1.5 cm³ lesion in the lung area, respectively.

Whether tracking an external point source or an internal region, the location estimate was always the one that minimized the sum of squared distances to all LORs that were within the selected ROI. Motion estimation from multiple point sources/internal regions was performed independently by selecting an ROI for each and using the set of LORs within that ROI. Table I provides additional details for all studies.

The point sources used consisted of zeolite beads (approximately 2 mm in diameter) soaked in an 18F-fluorodeoxyglucose solution for approximately 10 min. For the clinical studies with a single point source, it was placed on the center of the abdomen. For the clinical study with three point sources, they were placed on the center, left, and right side of the abdomen, approximately 13–18 cm apart from each other. Use of external markers for motion estimation has previously been studied.[46]

3. RESULTS

3.A. Analysis of extracted motion signals using TOF-PEPT

3.A.1 Studies with Anzai tracking system

Phantom Study 1: Point source and Anzai tracking: The range of movement observed in the estimated motion signal matched closely with the actual range of movement of the phantom. Furthermore, the signal correlated almost perfectly with the signal derived from Anzai band for the entire duration of the scan. Figure 1 provides a phase and displacement comparison between the motion signals derived from the

TABLE I. Description of the experimental studies conducted.

| Study	Anzai band used	Number of external point sources	Radioactivity (approx.) (kBq/mL)	Scan duration (min)	ROI circumradius (mm)
Phantom Study 1	Yes	1	Point Sources: 74–185	3	42.99
Phantom Study 2	No	1		15	17.59
Clinical Study 1	Yes	3		5	26.02, 21.71, 24.43
Clinical Study 2	Yes	1		3	24.28
Clinical Study 3	No	1		3	23.32
Clinical Study 4	No	1		3	31.10
Clinical Study 5	No	N/A		3	57.28
Clinical Study 6	No	N/A	Lesion: 10–15	3	24.39
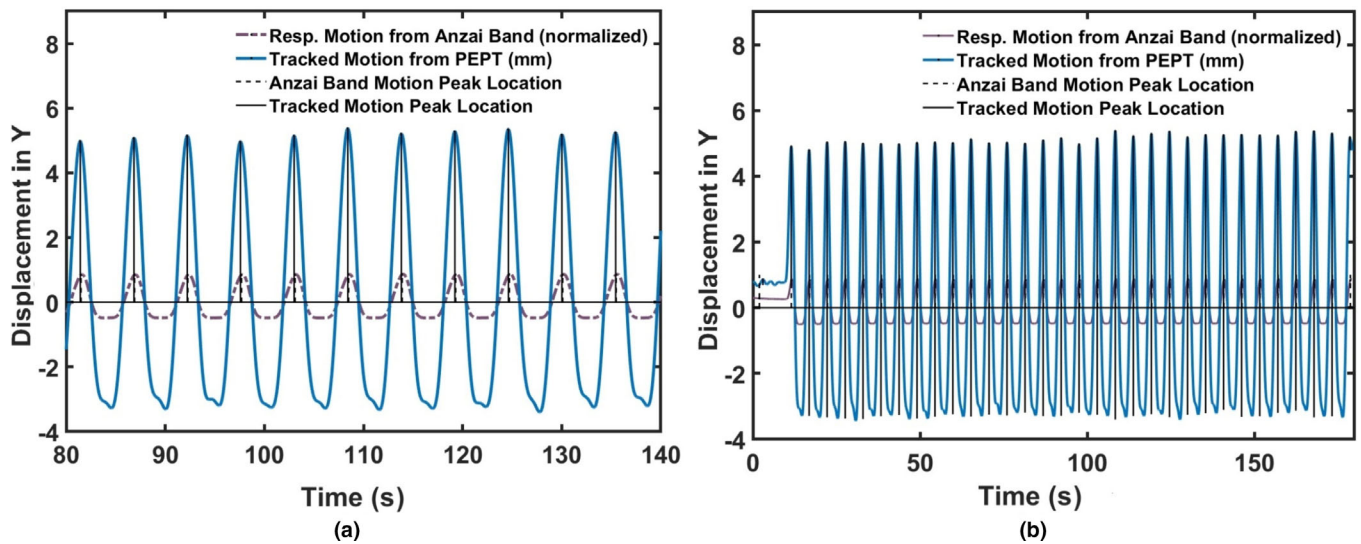
FIG. 1. Phase and displacement comparison of estimated motion signals by TOF-PEPT versus Anzai band for phantom study 1: (a) Displacement in Y for a 60-s time frame; (b) Displacement in Y for the full 3-min scan. For visualization purposes, the Anzai band data amplitude was normalized by its maximum value. The TOF-PEPT estimate was kept in the original mm-scale. The phase, displacement, and peak trigger location can be seen to correspond well. [Color figure can be viewed at wileyonlinelibrary.com]

Anzai band and the TOF-PEPT algorithm for the Y direction. Motion estimates for the Z direction correlated equally well.

Clinical Studies 1 and 2: Point sources and Anzai tracking: Figure 2 compares the Anzai band and TOF-PEPT motion estimates in the Y direction for one point source from Clinical Study 1. Between 20–30 s and 65–90 s, the patient incidentally moved, with the movement visible in both the Anzai band signal and the TOF-PEPT motion estimate. Compared with the sudden increase in the TOF-PEPT motion, the Anzai band signal appeared flattened, possibly due to

wraparound of measured values that exceeded the pressure thresholds of the sensor. The motion estimates for the two other point sources correlated equally well with the band as did the Clinical Study 2 estimates. A detailed quantitative comparison is provided in Section 3.C for both studies.

3.A.2. Studies without Anzai tracking system

Phantom Study 2: Point source and no Anzai tracking: A servo motor moved an arm with an attached point source up and down at three different frequencies for three different
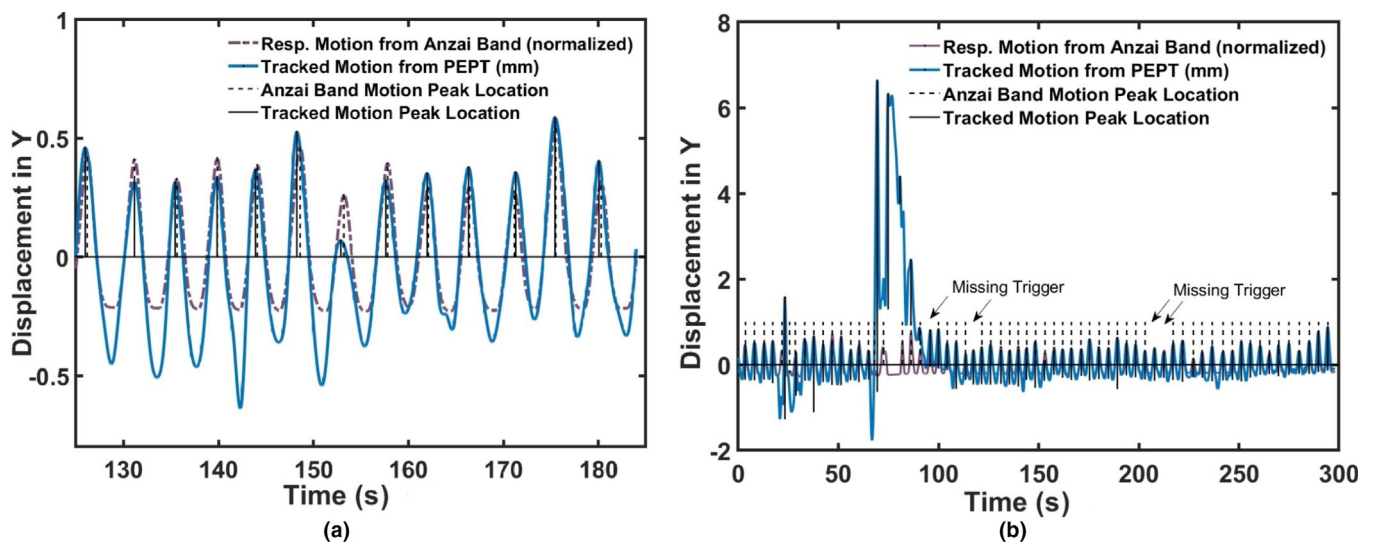

FIG. 2. Phase and displacement comparison of estimated motion signals by TOF-PEPT versus Anzai band for Clinical Study 1: (a) Displacement in Y for a 60-s time frame; (b) Displacement in Y for the full 5-min scan. For visualization purposes, the Anzai band data amplitude was normalized by its maximum value. The TOF-PEPT estimate was kept in the original mm-scale. Similarity in phase, displacement, and peak trigger location is evident except for a few places where there were unusual breathing patterns and missing trigger issues from the Anzai band. [Color figure can be viewed at wileyonlinelibrary.com]
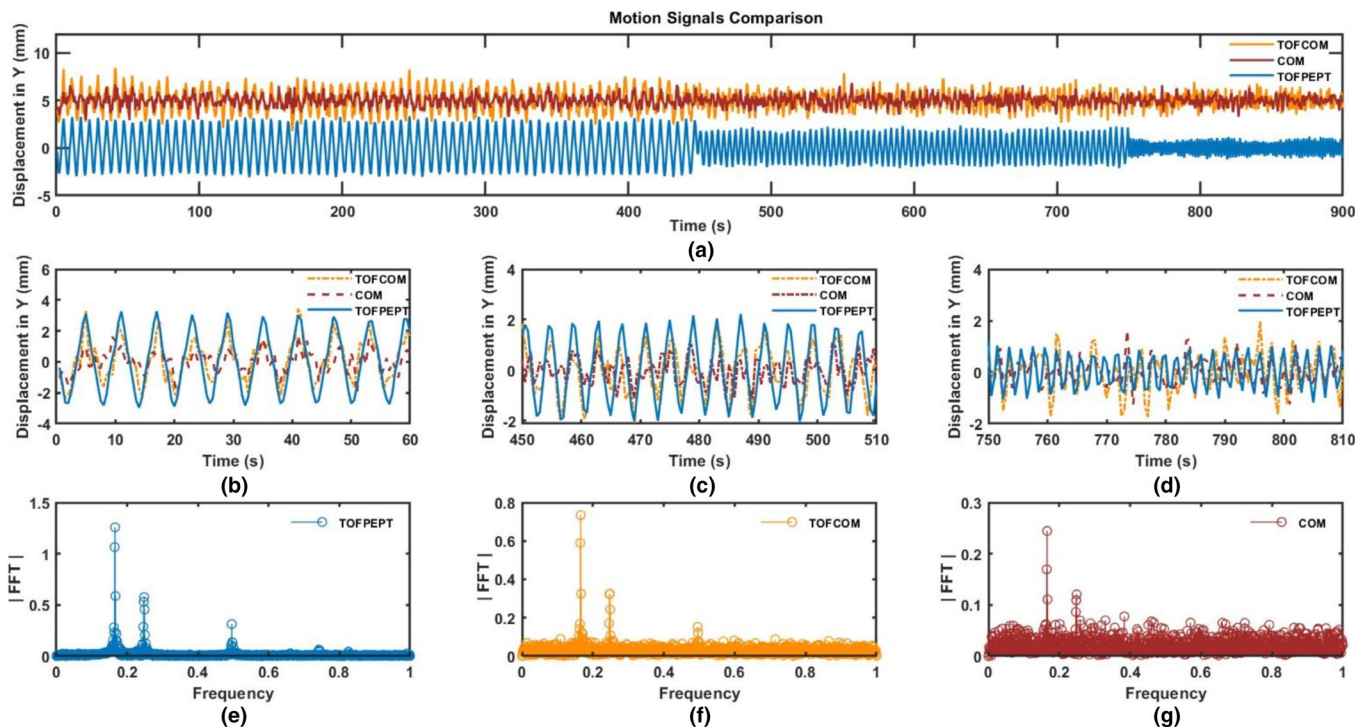
FIG. 3. Comparison of TOF-PEPT, TOF-COM, and COM estimated motion signals for Phantom Study 2: (a) Time domain plots for full 15-min scan with baseline shift added to the TOF-COM and COM signals for visualization purposes; (b)–(d) 60-s frames for the three different frequencies and amplitude ranges; (e)–(g) Fourier domain plots for full 15-min scan. [Color figure can be viewed at wileyonlinelibrary.com]

amplitude ranges. Figure 3 provides time and Fourier domain analysis of the estimated motion signals. The three frequencies are seen to be correctly identified by the TOF-PEPT algorithm with the signal suffering almost no random noise/fluctuations. Although the three frequencies were detected by the TOF-COM algorithm as well, the derived signals were noisier especially during the last segment where the phantom moved with the smallest amplitude range. Only the two lowest frequencies were identifiable by regular COM. Furthermore, the true range of displacement for the entire duration was successfully captured by TOF-PEPT only.

Clinical Studies 3 and 4: Point sources and no Anzai tracking: Figure 4 provides a visual comparison of the estimated motion signals in the time and Fourier domains for Clinical Study 3. The motion estimate obtained by the TOF-PEPT algorithm exhibited less noise compared with the COM algorithms. Similar results were obtained for Clinical Study 4.

Clinical Studies 5 and 6: Lesions/internal regions and no Anzai tracking: Here tracking was performed using data from regions selected within the patient to study the ability of the TOF-PEPT algorithm to estimate motion without use of a manufactured, external point source. Clinical Study 5 used the left cardiac ventricle. Clinical Study 6 used a small lesion in the lung area. Figures 5 and 6 provide time and Fourier domain plots of the corresponding motion signal estimates.

Figure 5 shows that the TOF-PEPT algorithm identified both the respiratory and the cardiac motion frequency components respectively at around 0.3 and 0.7 Hz. The latter was missing in the signals provided by the TOF-COM and COM algorithms. Figure 6 shows the lesion-specific motion estimate obtained by the TOF-PEPT algorithm to suffer less noise than those obtained by the TOF-COM and COM algorithms. The latter, in particular, was obscured by noise to the point of almost being undetectable.

3.B. Qualitative and quantitative comparison of gated images using signals from different methods

In this subsection, we present and evaluate the performance of each method in producing gating triggers and motion-compensated gated images for Clinical Study 1, which was based on motion estimation from a point source and the Anzai band, and Clinical Study 6, which was based on motion estimation from a lesion only.

Figure 7 compares images reconstructed using ungated data and data gated using motion estimates obtained with the Anzai band as well as the TOF-PEPT and COM algorithms for Clinical Study 1. Motion signals estimated from the point source placed on the center of the abdomen were used to gate the data. Data from after the patient's incidental movement during the scan were considered. The max SUV indicated for the lesion marked by an arrow shows that the uptake increased in the gated images with the max SUV being highest in the TOF-PEPT image; this SUV was higher than the
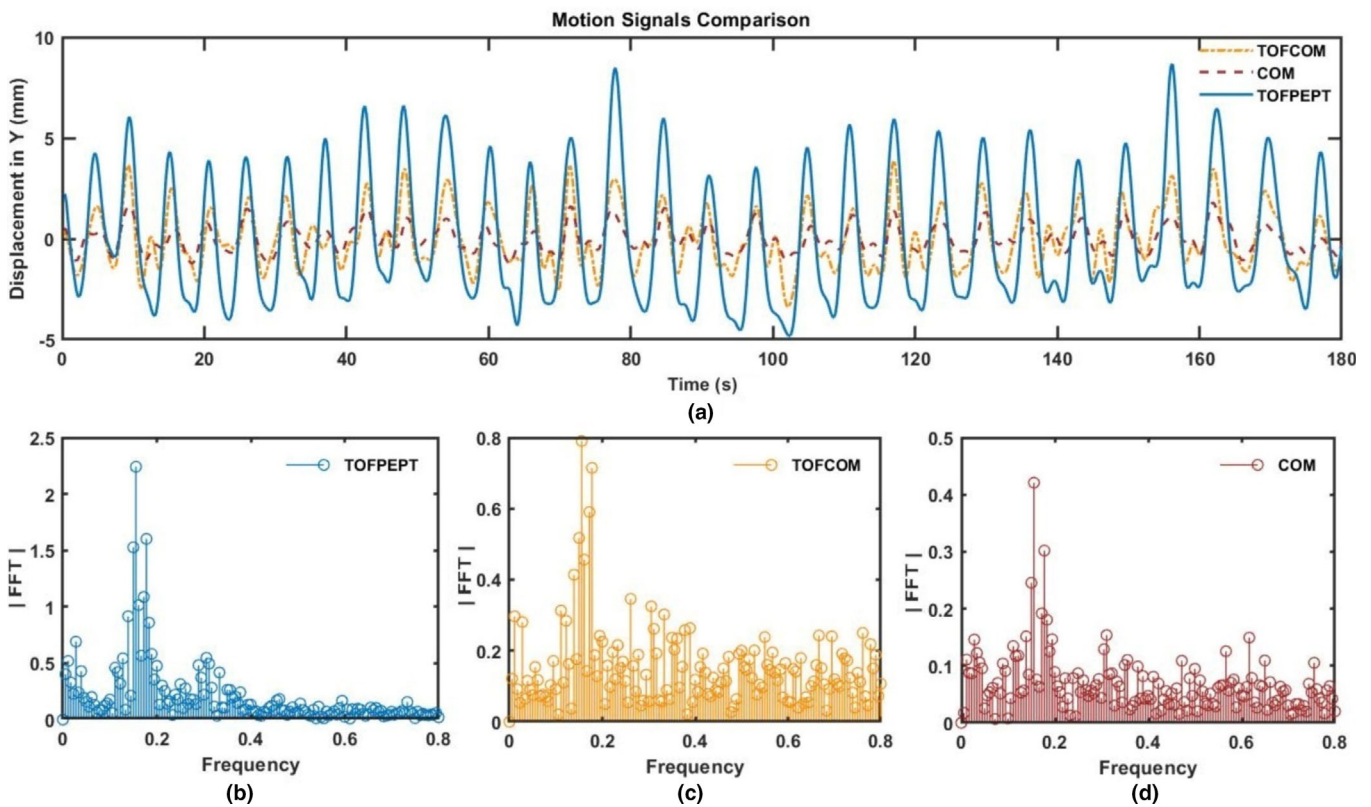
FIG. 4. Comparison of TOF-PEPT, TOF-COM, and COM estimated motion signals for Clinical Study 3: (a) Time domain plots; (b)–(d) Fourier domain plots. [Color figure can be viewed at wileyonlinelibrary.com]
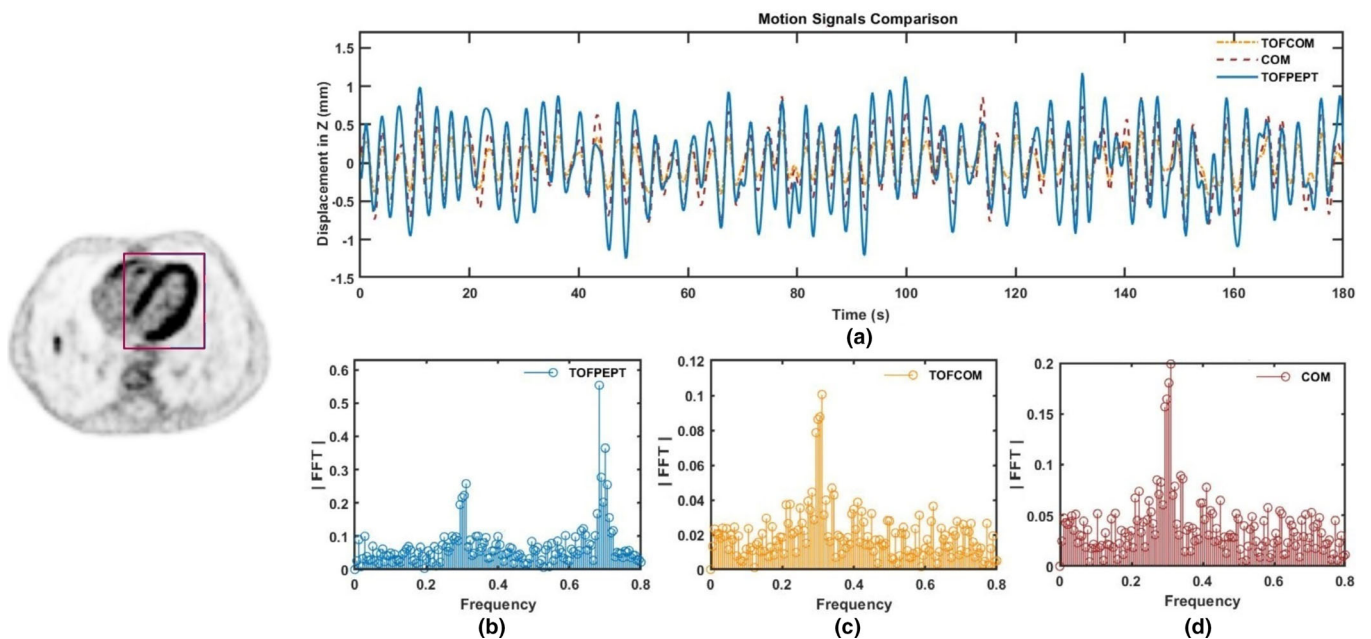

FIG. 5. Comparison of TOF-PEPT, TOF-COM, and COM estimated motion signals from left cardiac ventricle for Clinical Study 5: (a) Time domain plots showing only the respiratory motion by having applied a low pass filter with cutoff frequency of 0.5 Hz; (b)–(d) Fourier domain plots. [Color figure can be viewed at wileyonlinelibrary.com]

SUVs obtained for the ungated image by about 16% and the other gated images by 4–10%. A sole comparison with the ungated data showed an increase of 14–39% in maximum SUV across several lesions in the TOF gated data, depending on the amount of motion blurring that had occurred in that region.

Figure 8 compares ungated and gated images reconstructed using the lesion-specific motion estimates produced
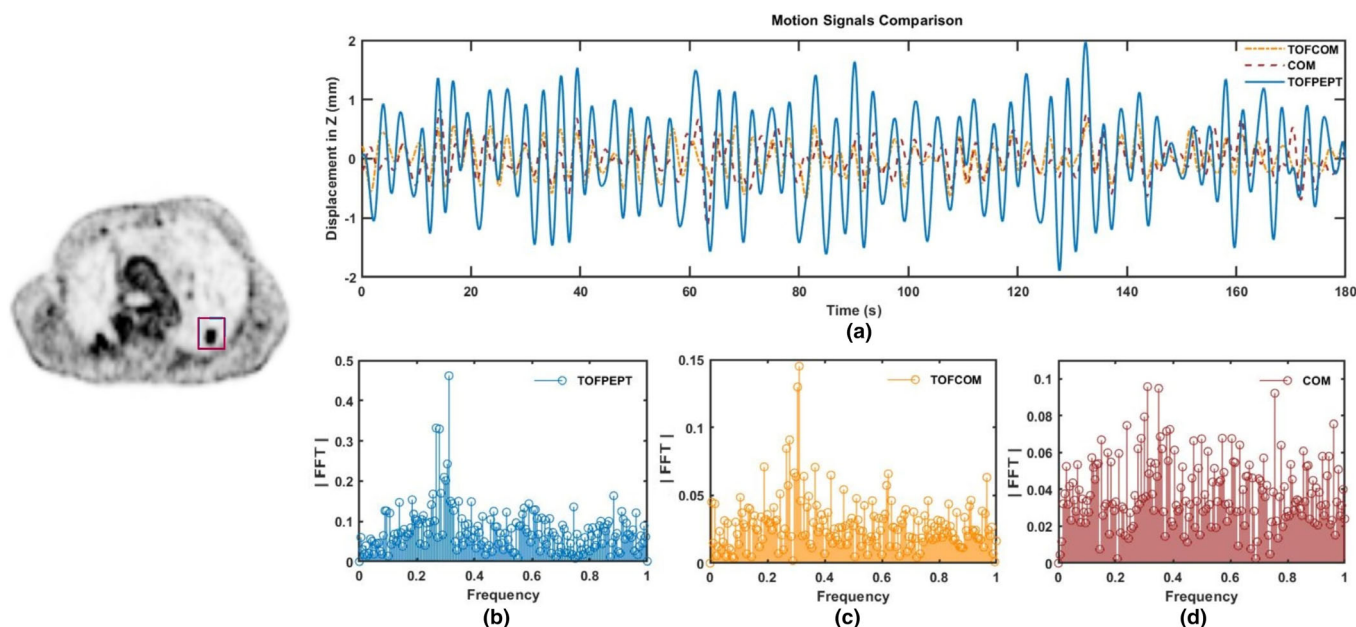
FIG. 6. Comparison of TOF-PEPT, TOF-COM, and COM estimated lesion-specific respiratory motion signals for Clinical Study 6: (a) Time domain plots; (b)–(d) Fourier domain plots. [Color figure can be viewed at wileyonlinelibrary.com]
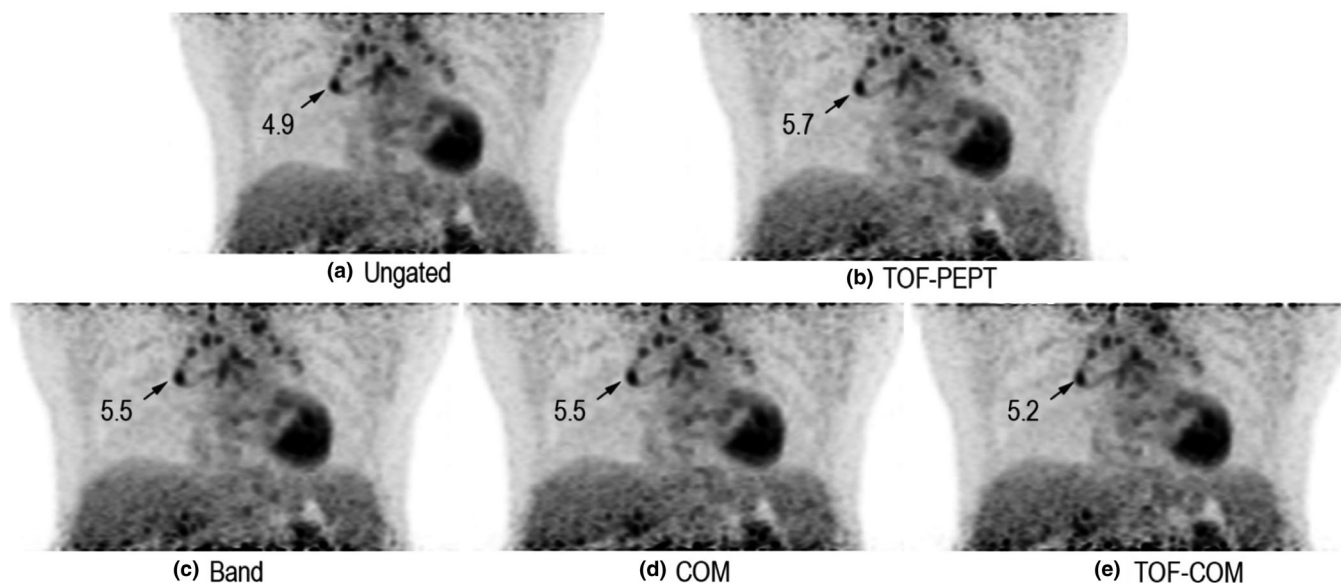

FIG. 7. Comparison of the (a) ungated and (b)–(e) amplitude-gated images for Clinical Study 1 using motion estimates based on TOF-PEPT, Anzai band, COM, and TOF-COM, respectively. Sharper images and increased maximum SUVs are observed in the data reconstructed using the signal from the TOF-PEPT algorithm.

by the TOF-PEPT, TOF-COM, and COM algorithms. The lesion can be seen more elongated and motion blurred in the ungated image as well as in the TOF-COM- and COM-gated images compared with the TOF-PEPT-gated image. This can also be seen from the Gaussian line profile fits provided for all four methods. FWHM across the lesion was lowest for the TOF-PEPT-based gated image. In comparison with the ungated image, a 12.17% reduction in FWHM was observed.

The maximum SUV was higher than the ungated, COM, and TOF-COM results by 8.7%, 7.1%, and 5.6%, respectively.

3.C. Quantitative comparison of extracted signals with Anzai respiratory band

Table II gives a quantitative comparison of the motion signals estimated by TOF-PEPT, TOF-COM, and COM with the
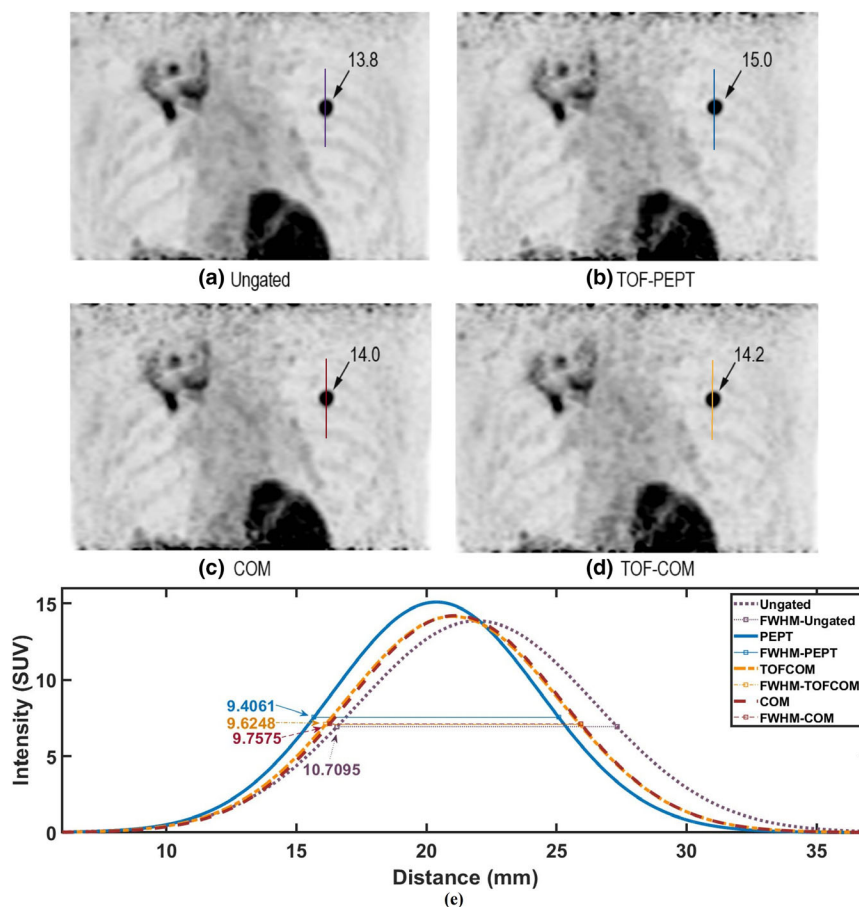
FIG. 8. Comparison of the (a) ungated and (b)–(d) amplitude-gated images for Clinical Study 6 using motion estimates based on TOF-PEPT, COM, and TOF-COM, respectively. The arrow indicates the maximum SUV in the lesion. (e) Result of Gaussian fitting applied to line profile data (a-d vertical lines). [Color figure can be viewed at wileyonlinelibrary.com]

TABLE II. Quantitative comparison of TOF-PEPT, COM, and TOF-COM estimated motion signals with Anzai band.

		Phantom	Clinical Study 1 (PS1[a])	Clinical Study 1 (PS2[a])	Clinical Study 1 (PS3[a])	Clinical Study 2
Correlation coefficient (CC)	TOF-PEPT	**0.995**	**0.966**	**0.94**	**0.947**	**0.976**
	TOF-COM	0.992	0.834	0.788	0.876	0.881
	COM	0.99	0.892	0.509	0.839	0.655
Root mean squared error (RMSE)	TOF-PEPT	**0.035**	**0.096**	**0.116**	**0.142**	**0.092**
	TOF-COM	0.078	0.148	0.183	0.217	0.144
	COM	0.056	0.138	0.203	0.228	0.229
Mean shift in peak locations (normalized)	TOF-PEPT	**0.002**	**0.017**	**0.021**	**0.026**	**0.019**
	TOF-COM	0.006	0.061	0.072	0.043	0.045
	COM	0.008	0.046	0.124	0.043	0.077

[a]PS1, PS2, and PS3 refer to point sources placed on center, left, and right respectively.
Values shown in bold indicate the highest correlation coefficient, and the lowest RMSE and mean shift in peak locations for each study.

Anzai band by means of the correlation coefficient (CC), the root mean squared error (RMSE), and the mean shift in peak location.

For Clinical Study 1, we used motion signals tracked from three point sources. For Clinical Study 2, we used the signal from a single point source. A frame duration of 500 ms was used in both cases. We compared the signals along the direction in which movement of the point sources was most significant, namely, the Y direction for the point sources placed on the center of abdomen, and the Z direction for the point sources placed on the side of the abdomen. TOF-PEPT exhibited the highest degree of correlation with the Anzai band, as well as, the lowest RMSE and mean shift in peak locations (shown in bold). There were average improvements of 13.5% and 38.7% in correlation compared to the TOF-COM and COM algorithms, respectively. For Clinical Study 1, TOF-PEPT performed notably better than TOF-COM and COM for one point source (PS2) that had relatively lower activity. We believe that the iterative process of selecting LORs and estimating the particle location led to better tracking than taking the average of all LORs within the ROI.

TABLE III. Implementation of PEPT under different conditions.

TOF-based LOR weighting	TOF-based LOR exclusion	Correlation coefficient (CC)				
		Phantom	Clinical Study 1 [a]PS1	Clinical Study 1 PS2	Clinical Study 1 PS3	Clinical Study 2
No	No	0.9946	0.9614	0.8986	0.9318	0.9665
No	Yes	0.9945	0.9580	0.8270	0.8960	0.9413
Yes	No	**0.9946**	**0.9661**	**0.9400**	**0.9468**	**0.9765**
Yes	Yes	0.9945	0.9592	0.8391	0.9015	0.9443

[a]PS: point source.
Values shown in bold indicate the highest correlation coefficient for each study.

Table III provides CCs with the Anzai band for TOF-PEPT implemented with/without TOF-based weighting (proposed in this paper) and with/without TOF-based LOR exclusion (proposed in the PeTrack paper). We observe that the highest CC values (shown in bold) were obtained with TOF-based weighting and no LOR exclusion. The opposite scenario produced the worst performance in every case. For the low activity point source (PS2) used in Clinical Study 1, TOF-based weighting produced a 4.6% increase in CC while TOF-based LOR exclusion caused a 7.9% decrease. We expect the improvement from TOF-based weighting to be even more significant for PET scanners that have better timing resolution than the one considered here.

3.D. Analysis of algorithm parameters

ROI size and frame duration were varied and the TOF-PEPT motion estimates were compared against the Anzai band. Figures 9 and 10 show the corresponding plots of CC, RMSE, and normalized mean shift of peak location. As the ROI was made larger, performance of the TOF-PEPT algorithm seems to degrade. We suspect that when the ROI becomes too large, LORs are included that do not pertain to the point source/lesion emissions. As for the frame duration, performance is negatively impacted both for short and for long time windows. The former is likely a result of not having enough LORs available while the latter is possibly due to the
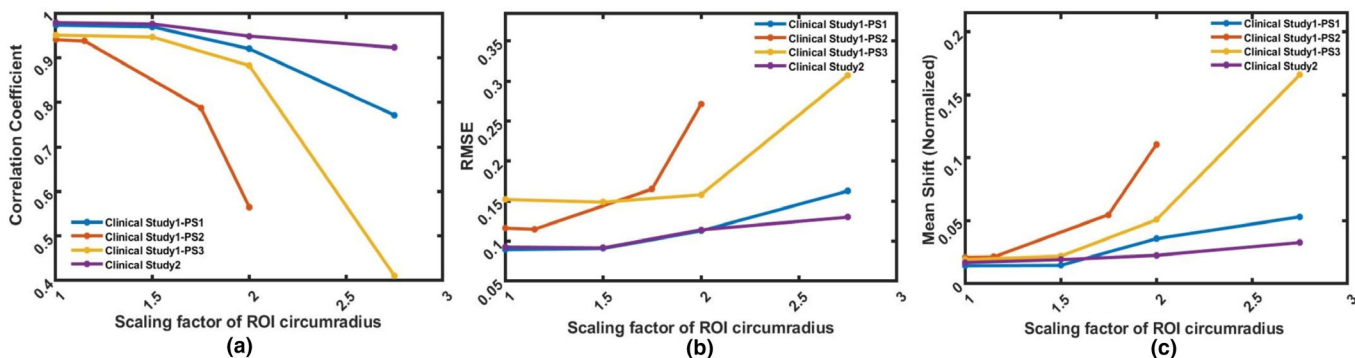

FIG. 9. Quantitative comparison of (a) correlation coefficient, (b) RMSE, and (c) normalized mean shift in peak location for different ROI circumradius scaling factors. Measurements degraded with increasing ROI size. Here, PS1, PS2, and PS3 indicate point sources placed on center, left, and right, respectively. [Color figure can be viewed at wileyonlinelibrary.com]
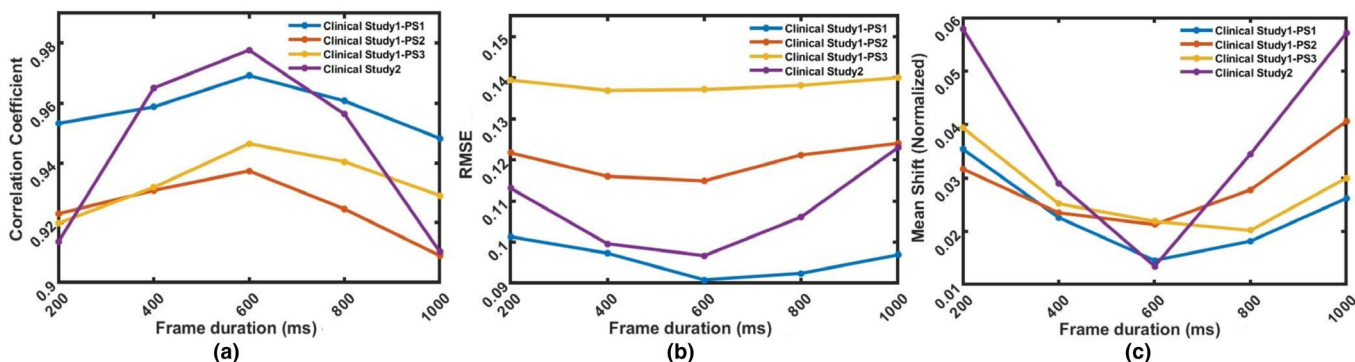

FIG. 10. Quantitative comparison of (a) correlation coefficient, (b) RMSE, and (c) normalized mean shift in peak location for different frame durations. Most favorable values lie in the range of 400–800 ms frame durations. Here, PS1, PS2, and PS3 indicate point sources placed on center, left, and right, respectively. [Color figure can be viewed at wileyonlinelibrary.com]

TABLE IV. Number of LORs and iterations for varying frame durations and ROI scaling factors.

Frame duration (ms)	Clinical Study 1		Clinical Study 2		ROI scaling factor	Clinical Study 1		Clinical Study 2	
	LORs (approx.)	Iterations	LORs (approx.)	Iterations		LORs (approx.)	Iterations	LORs (approx.)	Iterations
200	450	7	700	4	1	700	5	3000	4
400	800	7	2000	4	1.5	1000	7	4000	4
600	1200	7	3000	4	2	1800	8	5000	5
800	1500	7	4000	4	2.75	2400	9	8500	7
1000	2000	7	5000	4					

sampling rate being too low. These trends remained the same when the two parameters were varied simultaneously. Table IV shows the number of LORs considered and iterations needed with this varying parameter setup. We only show the numbers for a single point source for Clinical Studies 1 and 2. LOR count increased both for increasing frame duration and ROI size, whereas iteration count increased for latter only. This trend was observed for the other motion estimations as well.

4. DISCUSSION

The TOF-PEPT algorithm is a new data-driven approach for PET motion estimation that facilitates tracking of point sources as well as lesions and other internal regions directly from raw listmode data. Tracking accuracy was validated against an Anzai band, which is widely used in clinical studies. Comparison with two versions of a data-driven COM algorithm was also performed.

For studies performed with the Anzai band, the TOF-PEPT algorithm was found to produce motion estimates that correlated well with the band while outperforming the COM algorithms to varying degrees with respect to all quantitative and qualitative measures studied. For a frame duration of 500 ms, the motion signals from TOF-PEPT correlated with the band with CCs in the range of 0.94–0.97 for the clinical studies. In contrast, motion signals from the COM algorithms correlated with the band with CCs in the range of 0.51–0.92. For studies performed without the Anzai band, the TOF-PEPT motion estimates were found to be less noisy than the COM estimates both with respect to time and Fourier domain analysis in every case.

Reconstructed images generated from motion signals tracked using the TOF-PEPT algorithm also excelled when compared to the COM algorithms. Given the fact that all the gated images were subjected to similar count loss and noise characteristics from the use of amplitude-based gating methods, TOF-PEPT-based gated images showed a 6–9% increase in max SUV measured in lesions affected by motion.

The analysis with respect to frame duration and ROI size aided in studying the robustness of our algorithm. For 200 to 1000 ms frame durations, the TOF-PEPT algorithm provided good motion estimates with CCs in the range of 0.91–0.97. Tracked signals correlated with the band with CCs in the range of 0.88–0.97 up to the ROI circumradius scaling factor

of 2 except for one case with the low activity point source. Good tracking performance was thus achieved for a wide range of frame durations and ROI sizes.

The number of LORs considered and the number of iterations needed to do so varied with the ROI size and frame duration. As expected, the number of LORs increased almost linearly with larger ROIs and frame durations. More interestingly, the mean perpendicular distance from the LORs to the source particle/lesion increased in proportion to the size of the ROIs. This in turn increased the number of iterations required for the algorithm to discard more distant LORs. On the other hand, increasing the frame duration did not change the number of iterations needed. LORs were included in each frame in a way that did not affect much the mean perpendicular distance and thus the number of iterations.

Since the method allows tracking the motion along all the three axes at a time, it was possible to further study the principal axis of movement and its variation with respect to the point source/lesion/internal region location. Point sources placed on the abdomen showed principal movement in the Y direction, whereas point sources on the side of the abdomen showed movement mostly in the Z direction. The lung lesion and myocardium regions had their significant movements along Z direction. The ability to simultaneously track in all three dimensions facilitates use of the algorithm in body and head-neck studies since in such cases, the principal movement does not occur only in the axial direction.[21] Finally, the motion amplitude range observed with the TOF-PEPT algorithm matched the true range of motion more closely than the TOF-COM and COM algorithms.

An unexpected observation in comparing the other methods was that regular COM performed better than TOF-COM in one case. We had anticipated that use of TOF information would always lead to more precise tracking. With the TOF-COM algorithm using the average of the TOF annihilation location estimates within the ROI, large error/uncertainty may have affected performance. For the scanner used, the TOF FWHM was on the order of 6 cm and thus quite large compared to the 2 mm point source tracked. Another observation regarding the TOF-COM and COM algorithms was that they were found to be more sensitive to the ROI selection than the TOF-PEPT algorithm. In fact, the regular COM method could not provide satisfactory motion signal with the selected ROI for lesion motion tracking. The ROI size had to be decreased via further visual inspection in order to obtain a viable result.

We compared our TOF-based LOR weighting with the TOF-based exclusion implemented for the PeTrack algorithm. We observed that the LOR exclusion produced degraded performance in every case. In contrast, LOR weighting produced improved performance consistently. In particular, we noticed a 12.5% difference in CC when the point source had relatively lower activity (Clinical Study 1-Point Source 2). We speculate that hard-thresholding based on TOF (that has its own error in measurement) either removed LORs that should have been kept or caused LORs to be kept that should have been removed.

The proposed TOF-based weighting factor serves to emphasize the contribution of the more probable LORs. The more accurate the TOF information, the better the TOF-PEPT algorithm's ability to produce an accurate motion estimate. In this paper, we used data from a state-of-the-art photomultiplier (PMT)-based PET/CT system. Next generation SiPM-based PET systems should increase LOR position accuracy with their improved TOF measurement capabilities.

We have shown successful lesion-specific motion tracking based on activity concentrations of 10–30 kBq/mL. Adding additional data corrections, such as attenuation correction and scatter correction, may help improve the lower limits of detection as well as the positional accuracy. This is the focus of future work along with further validation in routine clinical use and characterization across a wider range of imaging conditions than considered here.

5. CONCLUSIONS

Respiratory motion negatively impacts PET/CT images both qualitatively and quantitatively. Most hardware and data-driven motion tracking methods only serve to estimate external and global respiratory motion patterns. A global motion estimate may not fully capture lesion-specific/localized internal motion. The presented TOF-PEPT algorithm provides a framework for more accurate estimation of lesion/internal region motion for use by reconstruction algorithms and event-by-event motion correction. The scope of the work was to investigate feasibility of the proposed technique when applied to data obtained from a standard clinical PET/CT imaging system with emphasis on respiratory gating and lesion/internal region motion tracking. We compared performance against a standard Anzai band as well as two COM algorithms. The TOF-PEPT algorithm was found to produce results that were equivalent to the Anzai band and better than the COM algorithms. We have shown that lesion-specific tracking can be performed, which may have applications in routine clinical PET/CT, radiation therapy planning, as well as for providing more robust tracking information for use in fine-tuning motion correction algorithms.

CONFLICT OF INTEREST

To the best of the authors' knowledge, there is no conflict to disclose.

a)Author to whom correspondence should be addressed. Electronic mail: ttumpa@vols.utk.edu.

REFERENCES

1. Dawood M, Lang N, Jiang X, Schafers KP. Lung motion correction on respiratory gated 3-D PET/CT images. *IEEE Trans Med Imaging*. 2006;25:476–485.
2. Dawood M, Buther F, Jiang X, Schafers KP. Respiratory motion correction in 3-D PET data with advanced optical flow algorithms. *IEEE Trans Med Imaging*. 2008;27:1164–1175.
3. Qiao F, Pan T, Clark JW Jr, Mawlawi OR. A motion-incorporated reconstruction method for gated PET studies. *Phys Med Biol*. 2006;51:3769–3783.
4. Lamare F, Fayad H, Fernandez P, Visvikis D. Local respiratory motion correction for PET/CT imaging: application to lung cancer. *Med Phys*. 2015;42:5903–5912.
5. Liu C, Alessio AM, Kinahan PE. Respiratory motion correction for quantitative PET/CT using all detected events with internal-external motion correlation. *Med Phys*. 2011;38:2715–2723.
6. Klein G, Reutter B, Botvinick E, Budinger T, Huesman R. Fine-scale motion detection using intrinsic list mode PET information. IEEE Workshop on Mathematical Methods in Biomedical Image Analysis:71–78. IEEE; 2001.
7. Bundschuh RA, Martinez-Moeller A, Essler M, et al. Postacquisition detection of tumor motion in the lung and upper abdomen using list-mode PET data: a feasibility study. *J Nucl Med*. 2007;48:758–763.
8. Thielemans K, Rathore S, Engbrant F, Razifar P. Device-less gating for PET/CT using PCA. 2011 IEEE Nuclear Science Symposium 3904-3910. IEEE; 2011.
9. Visvikis D, Barret O, Fryer T, et al. A posteriori respiratory motion gating of dynamic PET images. 2003 IEEE Nuclear Science Symposium. Conference Record (IEEE Cat. No.03CH37515):3276–3280. IEEE; 2003.
10. Schleyer PJ, O'Doherty MJ, Barrington SF, Marsden PK. Retrospective data-driven respiratory gating for PET/CT. *Phys Med Biol*. 2009;54:1935–1950.
11. Schleyer PJ, O'Doherty MJ, Marsden PK. Extension of a data-driven gating technique to 3D, whole body PET studies. *Phys Med Biol*. 2011;56:3953.
12. Kesner AL, Bundschuh RA, Detorie NC, et al. Respiratory gated PET derived in a fully automated manner from raw PET data. *IEEE Trans Nucl Sci*. 2009;56:677–686.
13. Kesner AL, Kuntner C. A new fast and fully automated software based algorithm for extracting respiratory signal from raw PET data and its comparison to other methods. *Med Phys*. 2010;37:5550–5559.
14. He J, O'Keefe GJ, Gong SJ, et al. A novel method for respiratory motion gated with geometric sensitivity of the scanner in 3D PET. *IEEE Trans Nucl Sci*. 2008;55:2557–2565.
15. Buther F, Dawood M, Stegger L, et al. List mode-driven cardiac and respiratory gating in PET. *J Nucl Med*. 2009;50:674–681.
16. Büther F, Vehren T, Schäfers KP, Schäfers M. Impact of data-driven respiratory gating in clinical PET. *Radiology*. 2016;281:229–238.
17. Sorenson JA, Phelps ME. *Physics in Nuclear Medicine*. New York: Grune & Stratton; 1987.
18. Vandenberghe S, Mikhaylova E, D'Hoe E, Mollet P, Karp JS. Recent developments in time-of-flight PET. *EJNMMI Phys*. 2016;3:3.
19. Ren S, Jin X, Chan C, et al. Data-driven event-by-event respiratory motion correction using TOF PET list-mode centroid of distribution. *Phys Med Biol*. 2017;62:4741–4755.
20. Ren S, Lu Y, Bertolli O, Thielemans K, Carson RE. Event-by-event non-rigid data-driven PET respiratory motion correction methods: comparison of principal component analysis and centroid of distribution. *Phys Med Biol*. 2019;64:165014.
21. Lu Y, Gallezot J-D, Naganawa M, et al. Data-driven voluntary body motion detection and non-rigid event-by-event correction for static and dynamic PET. *Phys Med Biol*. 2019;64:065002.
22. Xu J, Tsui BM. Improved intrinsic motion detection using time-of-flight PET. *IEEE Trans Med Imaging*. 2015;34:2131–2145.

23. Feng T, Wang J, Sun Y, Zhu W, Dong Y, Li H. Self-gating: an adaptive center-of-mass approach for respiratory gating in PET. *IEEE Trans Med Imaging*. 2017;37:1140–1148.

24. Salomon A, Zhang B, Olivier P, Goedicke A. Robust real-time extraction of respiratory signals from PET list-mode data. *Phys Med Biol*. 2018;63:115009.

25. Bertolli O, Arridge S, Stearns CW, Wollenweber SD, Hutton BF, Thielemans K. Data driven respiratory signal detection in PET taking advantage of time-of-flight data. 2016 IEEE Nuclear Science Symposium, Medical Imaging Conference and Room-Temperature Semiconductor Detector Workshop (NSS/MIC/RTSD):1-3. IEEE; 2016.

26. Bertolli O, Arridge S, Wollenweber SD, Stearns CW, Hutton BF, Thielemans K. Sign determination methods for the respiratory signal in data-driven PET gating. *Phys Med Biol*. 2017;62:3204.

27. Walker MD, Bradley KM, McGowan DR. Evaluation of principal component analysis-based data-driven respiratory gating for positron emission tomography. *Br J Radiol*. 2018;91:20170793.

28. Wang M, Guo N, Zhang H, Elfhakri G, Hu G, Li Q. Retrospective data-driven respiratory gating for PET using TOF information. 2015 37th Annual International Conference of the IEEE Engineering in Medicine and Biology Society (EMBC):4520-4523. IEEE; 2015.

29. Wang M, Guo N, Schaefferkoetter J, et al. Automatic respiratory gating of TOF-PET data using time-of-flight information. *J Nucl Med*. 2015;56:427.

30. Parker D, Dijkstra A, Martin T, Seville J. Positron emission particle tracking studies of spherical particle motion in rotating drums. *Chem Eng Sci*. 1997;52:2011–2022.

31. Parker DJ, Fan X. Positron emission particle tracking—application and labelling techniques. *Particuology*. 2008;6:16–23.

32. Bakalis S, Fryer P, Parker D. Measuring velocity distributions of viscous fluids using positron emission particle tracking (PEPT). *AIChE J*. 2004;50:1606–1613.

33. Osborne DR, Hu D, Lee SH. Inventors; Google Patents. Motion correction for PET medical imaging based on tracking of annihilation photons. US patent US 10,255,684 B2 2019.

34. Tumpa TR, Acuff SN, Gregor J, Lee S, Hu D, Osborne DR. Respiratory Motion Correction Using A Novel Positron Emission Particle Tracking Technique: A Framework Towards Individual Lesion-Based Motion Correction. 2018 40th Annual International Conference of the IEEE Engineering in Medicine and Biology Society (EMBC):5249-5252. IEEE; 2018.

35. Osborne D, Acuff S, Tumpa T, Hu D. Respiratory motion correction using novel particle tracking techniques. *J Nucl Med*. 2017;58:1362.

36. Osborne D, Hyeb Lee S, Hu D, Acuff S. Head and neck motion correction in PET imaging using new particle tracking techniques. *J Nucl Med*. 2015;56:1822.

37. Chamberland MJ, deKemp RA, Xu T. Motion tracking of low-activity fiducial markers using adaptive region of interest with list-mode positron emission tomography. *Med Phys*. 2020;47:3402–3414.

38. Manwell S, Klein R, Xu T, deKemp RA. Clinical comparison of the positron emission tracking (PeTrack) algorithm with the real-time position management system for respiratory gating in cardiac positron emission tomography. *Med Phys*. 2020;47:1713–1726.

39. Conti M, Bendriem B. The new opportunities for high time resolution clinical TOF PET. *Clin Translat Imaging*. 2019;7:139–147.

40. Jakoby B, Bercier Y, Conti M, Casey M, Bendriem B, Townsend D. Physical and clinical performance of the mCT time-of-flight PET/CT scanner. *Phys Med Biol*. 2011;56:2375.

41. Karlberg AM, Sæther O, Eikenes L, Goa PE. Quantitative comparison of PET performance—Siemens biograph mCT and mMR. *EJNMMI Phys*. 2016;3:5.

42. Franssen T. *Verification of the spatial and timing resolution of the Siemens TOF-PET detector based on the Biograph mCT Flow*: Bachelor's Thesis, Physics, University of Groningen; 2018.

43. Hamill JJ, Le Meunier L, Inventors; Google Patents. Optimal respiratory gating in medical imaging. US patent US 9,579,070 B2 2017.

44. Medixant. RadiAnt DICOM Viewer. https://www.radiantviewer.com

45. Arduino. https://www.arduino.cc/

46. Büther F, Ernst I, Hamill J, et al. External radioactive markers for PET data-driven respiratory gating in positron emission tomography. *Eur J Nucl Med Mol Imaging*. 2013;40:602–614.